Luminescent Ag-doped In2S3 nanoparticles stabilized by mercaptoacetate in water and glycerol

ARTICLE *in* JOURNAL OF NANOPARTICLE RESEARCH · MARCH 2015

Impact Factor: 2.18 · DOI: 10.1007/s11051-015-2953-1

5 AUTHORS, INCLUDING:

Alexandra Raevskaya

National Academy of Sciences of Ukraine

83 PUBLICATIONS **617** CITATIONS

SEE PROFILE

Oleksandr L. Stroyuk

L.V. Pisarzhevskiy Institute Of Physical Che…

145 PUBLICATIONS **1,067** CITATIONS

SEE PROFILE

Victor F Plyusnin

Institute of Chemical Kinetics and Cobustio…

160 PUBLICATIONS **1,084** CITATIONS

SEE PROFILE

Luminescent Ag-doped In_2S_3 nanoparticles stabilized by mercaptoacetate in water and glycerol

Alexandra E. Raevskaya, Maria V. Ivanchenko, Oleksandr L. Stroyuk, Stepan Ya. Kuchmiy & Victor F. Plyusnin

Journal of Nanoparticle Research
An Interdisciplinary Forum for
Nanoscale Science and Technology

ISSN 1388-0764
Volume 17
Number 3

J Nanopart Res (2015) 17:1-12
DOI 10.1007/s11051-015-2953-1

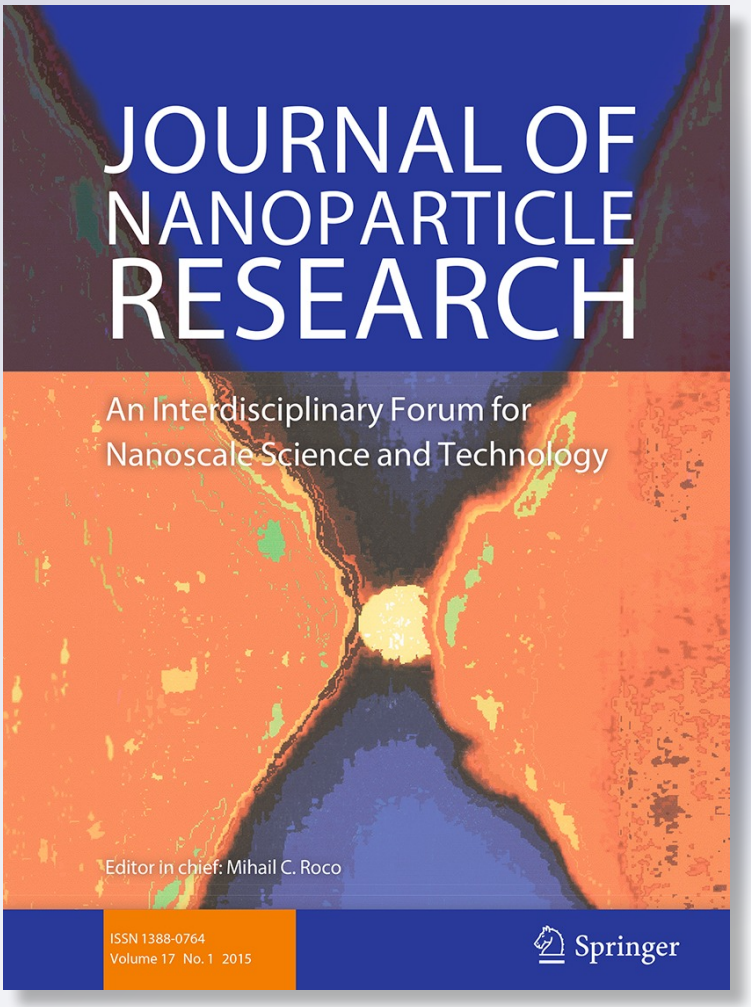

Springer

J Nanopart Res (2015) 17:135
DOI 10.1007/s11051-015-2953-1

RESEARCH PAPER

Luminescent Ag-doped In_2S_3 nanoparticles stabilized by mercaptoacetate in water and glycerol

Alexandra E. Raevskaya · Maria V. Ivanchenko · Oleksandr L. Stroyuk · Stepan Ya. Kuchmiy · Victor F. Plyusnin

Received: 2 December 2014 / Accepted: 6 March 2015

Abstract Colloidal nanoparticles (NPs) of tetragonal β-In_2S_3 were stabilized in water and glycerol by mercaptoacetate anions. Doping of In_2S_3 NPs with Ag^I cations at the time of the synthesis imparts the NPs with the photoluminescence (PL) in the visible part of the spectrum. The doping results also in a shift of the absorption threshold and the PL band maximum to longer wavelengths proportional to the Ag^I content. The PL band maximum of Ag^I-doped In_2S_3 NPs can be varied from 575–580 to 760–765 nm by augmenting the silver(I) amount and the duration and temperature of the post-synthesis aging. The average radiative life-time of Ag^I-doped In_2S_3 NPs also depends on the silver(I) content and reaches the maximal value, 960 ns, at a molar Ag:In ratio of 1:4. The maximal quantum yield of stationary PL, 12 %, is observed at this Ag:In ratio as well. Deposition of a ZnS "shell" on the surface of Ag^I-doped In_2S_3 NPs results in an increase of the PL quantum yield to $\sim$30 %.

Keywords I–III–VI_2 compounds · Indium sulfide · Silver indium sulfide · Time-resolved photoluminescence · Optical properties · Colloids

Electronic supplementary material The online version of this article (doi:10.1007/s11051-015-2953-1) contains supplementary material, which is available to authorized users.

A. E. Raevskaya · M. V. Ivanchenko · O. L. Stroyuk (✉) · S. Ya. Kuchmiy
Department of Photochemistry, L.V. Pysarzhevsky Institute of Physical Chemistry of National Academy of Sciences of Ukraine, 31 Nauky Av., Kiev 03028, Ukraine
e-mail: alstroyuk@ukr.net; stroyuk@inphyschem-nas.kiev.ua

V. F. Plyusnin
Institute of Chemical Kinetics and Combustion of Siberian Branch of Russian Academy of Sciences, Novosibirsk, Russian Federation

V. F. Plyusnin
Novosibirsk State University, Novosibirsk, Russian Federation

Introduction

Among the semiconductor nanoparticles (NPs) that can be applied as photochemically stable luminophores or photosensitive components of solar cells, the leading positions belonged for a long time to cadmium and lead chalcogenides—CdX and PbX, X = S, Se, Te (Klostranec and Chan 2006; Kamat et al. 2010; Rühle et al. 2010; Talapin et al. 2010). Recent years have been marked by an active search of new semiconductor NPs comparable to CdX and PbX by the luminescent and/or photochemical properties. The search has resulted in a progress in the studies of ternary I–III–VI_2 compounds, in particular $CuInS_2$, $AgInS_2$, and related solid solutions (Zhong et al. 2012; Kolny-Olesiak and Weller 2013; Torimoto et al. 2014). Such compounds are characterized by a strong

Published online: 13 March 2015

dependence of spectral and luminescent properties on the NP size and composition. At the same time, such NPs retain the crystal structure unchanged after abundant doping with metal ions resulting in considerable deviation from the stoichiometry. These properties of ternary In-based NPs open opportunities for the design of four- to five-component solid solutions and broad variation of the range of light absorption and emission (Zhong et al. 2012; Kolny-Olesiak and Weller 2013; Torimoto et al. 2014). In this direction, the major attention is drawn to $CuInS_2$ NPs (Kolny-Olesiak and Weller 2013), while structurally similar NPs of $AgInS_2$ and related non-stoichiometric solid solutions remain studied to a much lesser extent.

The I–III–VI_2 NPs, in particular silver indium sulfide and related solid solution produced by the chemical bath deposition (Chang et al. 2010; Li et al. 2013), thermal decomposition of a single-molecule precursor (Sasamura et al. 2012), microwave (Zhang et al. 2011; Xiong et al. 2013) and hydrothermal (Du et al. 2007; Yin et al. 2013; Han et al. 2014) treatment, etc., exhibit broad absorption bands in the visible part of the spectrum. Such NPs are currently applied as luminophores (Xiong et al. 2013), spectral sensitizers of the wide-bandgap oxide photoanodes of the solar cells (Chang et al. 2010; Yin et al. 2013; Han et al. 2014), and as photocatalysts and components of heterostructured photocatalysts (Zhang et al. 2011; Li et al. 2013).

Colloidal $AgInS_2$ and "core/shell" $AgInS_2$/ZnS NPs (Du et al. 2007; Tian and Vittal 2007; Li et al. 2010; Chang et al. 2012; Liu et al. 2013; Xiong et al. 2013; Torimoto et al. 2012, 2014; Hamanaka et al. 2014; Xiang et al. 2014) as well as non-stoichiometric Ag–In–S compounds and the solid solution ZnS–$AgInS_2$ NPs (Sasamura et al. 2012; Tang et al. 2012; Peng et al. 2013; Rao et al. 2014; Torimoto et al. 2010, 2014; Xiang et al. 2014) are typically produced by the well-known "hot injection" methods and often demonstrate high quantum yields (QY) of the photoluminescence (PL)—up to 80 % (Torimoto et al. 2010). Along with high PLQY, such NPs combine the photochemical stability with versatility of the means of tailoring of the PL band maximum position from 400 to 800 nm via variation in the NP size and composition. Owing to these beneficial properties, the Ag–In–S family NPs are currently intensely explored as luminescent biomarkers (Chang et al. 2012; Tang et al. 2012; Liu et al. 2013; Peng et al. 2013; Hamanaka et al. 2014).

Successful application of luminescent I–III–VI_2 NPs, including Ag–In–S systems, as luminescent biolabels requires stabilization of such NPs in polar media. At the same time, no reports on the synthesis of luminescent Ag–In–S NPs in polar solvents including water can be found in literature. In this connection, the present paper focuses on the synthesis of indium(III) sulfide NPs stabilized by mercaptoacetate anions in water and glycerol, luminescent properties of In_2S_3 NPs doped with Ag^I ions (Ag–In–S NPs), as well as the effects of NP composition, the post-synthesis aging, and deposition of a zinc sulfide "shell" on the spectral and PL characteristics of the non-stoichiometric Ag–In–S NPs.

Materials and methods

Indium(III) chloride, silver(I) nitrate, $Na_2S \times 9H_2O$, NaOH, mercaptoacetic acid (MAA), and anthracene (ultrapure) were purchased from Sigma Aldrich and used without any further purification. Stock solutions used in the NP synthesis were aqueous 0.1 M $AgNO_3$, 1.0 M NaOH, 1.0 M MAA, 1.0 M $InCl_3$, 0.1 M Na_2S, and 1.0 M $Zn(CH_3COO)_2$ solutions. To prevent hydrolysis of In^{3+} and Zn^{2+} ions, 0.2 M and 0.01 M HNO_3, respectively, were introduced to the indium(III) chloride and zinc(II) acetate stock solutions.

Colloidal In_2S_3 NPs were synthesized at room temperature via interaction between $InCl_3$ and Na_2S in aqueous or glycerol solution of sodium mercaptoacetate. In a typical procedure, 0.15 mL stock NaOH solution and 0.15 mL stock MAA solution were added to 8.9 mL distilled water or glycerol under stirring. 0.04 mL stock $InCl_3$ solution and 0.7 mL of freshly prepared stock solution of Na_2S were added to the mixture under vigorous stirring. Finally, 0.05 mL stock MAA solution was added to the colloid.

Silver(I)-doped colloidal In_2S_3 NPs (denoted further as Ag–In–S NPs) were synthesized via interaction between a mixture of mercaptoacetate complexes of Ag^I and In^{III} with Na_2S in water or glycerol at room temperature. In a typical procedure, 0.1 mL stock solution of $AgNO_3$, 0.15 mL stock solution of NaOH, and 0.15 mL stock solution of MAA were added to 8.9 mL distilled water or glycerol under stirring. 0.04 mL stock solution of $InCl_3$ and 0.7 mL of freshly prepared stock solution of Na_2S were added to the homogenized mixture under vigorous stirring. The

synthesis was finalized by the addition of 0.05 mL stock MAA solution. The colloidal Ag–In–S solutions were kept in sealed vessels to avoid oxidation of MAA.

To achieve the maximal PL quantum yield, the solutions were kept at room temperature for 5–7 days or subjected to a thermal treatment at ~100 °C for 15 min. Keeping the Ag:In ratio constant, the molar concentration of Ag–In–S can be raised up to 1×10^{-2} M without noticeable changes of the optical characteristics of Ag–In–S NPs.

Zinc sulfide was deposited on the Ag–In–S NPs using the procedure similar to that applied by us earlier to produce "core/shell" CdSe/ZnS NPs (Dzhagan et al. 2008, 2009). 0.1 mL stock MAA solution and 0.1 mL stock NaOH solution were added to 10 mL of the Ag–In–S colloid. Then 0.14 mL stock zinc(II) acetate was introduced to the mixture under vigorous stirring followed by 0.1 mL 1.0 M Na_2S solution. The solutions were then kept at room temperature for 5–7 days or subjected to thermal treatment at ~100 °C for 15 min to complete formation of a ZnS shell and to achieve the maximal PLQY.

Purification of colloidal solutions was performed by dialysis against distilled water for 24 h using CelluSep H1 membranes (1 kDa, Orange Scientific).

The absorption spectra were registered with an HP Agilent 8453 spectrophotometer. The bandgap of In_2S_3 and Ag–In–S NPs was determined from the absorption band edge position using Tauc equation $\alpha = A(h\nu - E_g)^n$, where α is an absorption coefficient proportional to the optical density D, A is a constant, $h\nu$ is a quantum energy, and $n = ½$ and 2 for allowed direct and indirect interband electron transitions, respectively.

The PL spectra and PL decay curves were obtained using an Edinburgh Instruments FLS920 photon counting system. The PLQY was estimated using solid ultrapure anthracene (PLQY = 100 %) as a reference. A diode EPL-375 laser emitting 60-ps pulses with $\lambda = 375$ nm was used to excite the samples placed in standard 1.0 mm quartz cuvettes. The Stokes shift of the emission band maximum was determined as the difference between the minimal energy of electron transition in NPs and the energy corresponding to the PL band maximum.

The PL decay curves were approximated by a linear combination of 3 monoexponential functions $I(t) = \sum_i A_i e^{-t/\tau_i}$, where I is the PL intensity, $i = 1$–3, with the amplitudes A_i and times τ_i as the fitting parameters. The average PL decay time $<\tau>$ was determined as $<\tau> = \sum_i \frac{A_i \tau_i^2}{\sum_j A_j \tau_j}$. Dynamic light-scattering (DLS) measurements were performed with a Zetasizer Nano (Malvern Instruments). Transmission electron microscopy (TEM) and high-resolution TEM (HRTEM) studies were performed on a Selmi PEM-125K (accelerating voltage of 100 kV) and a Philips CM 20 FEG microscope (accelerating voltage of 200 kV), respectively. Scanning electron microscopic (SEM) images were taken on a Mira 3 Tescan LMU microscope coupled with an Oxford X-max 80 mm^2 setup for the energy-dispersive X-ray spectroscopy (EDX) at accelerating voltages of 10–20 kV.

Results and discussion

Structure and optical properties of mercaptoacetate-stabilized colloidal In_2S_3 NPs

The absorption spectrum of aqueous indium(III) sulfide colloid stabilized by mercaptoacetate (MA) anions reveals a continuous band with an edge at ~320 nm (Fig. 1a). The spectral curve is linear when plotted as $(D \times h\nu)^{0.5}$ versus $h\nu$ in the range of $h\nu > 3.8$–3.9 eV (Fig. 1a, inset) indicating that the light absorption near the band edge of the colloidal solution originates from an indirect interband electron transition in In_2S_3 NPs. A minimal energy E_i of the transition, determined as a cross point between a tangent to the linear section and the abscissae axis, is 3.68 ± 0.01 eV. The value is much larger than the bandgap of bulk tetragonal In_2S_3, ~2 eV (Nagesha et al. 2001; Park et al. 2006), indicating that the photogenerated charge carriers experience spatial confinement in In_2S_3 NPs and that the NP size is smaller than the doubled Bohr exciton radius in In_2S_3, ~60 nm (Chen et al. 2004). It should be noted that the In_2S_3 NPs stabilized by MA in water and glycerol have identical spectral properties.

The bright-field TEM shows that colloidal solutions of MA-stabilized indium(III) sulfide in water contain polydisperse NPs with a size of 15–30 nm (Electronic Supplementary Materials (ESM), Fig. S1a). The selected-area electron diffraction (SAED) pattern of In_2S_3 NPs (Fig. S1b) reveals concentric reflections of a

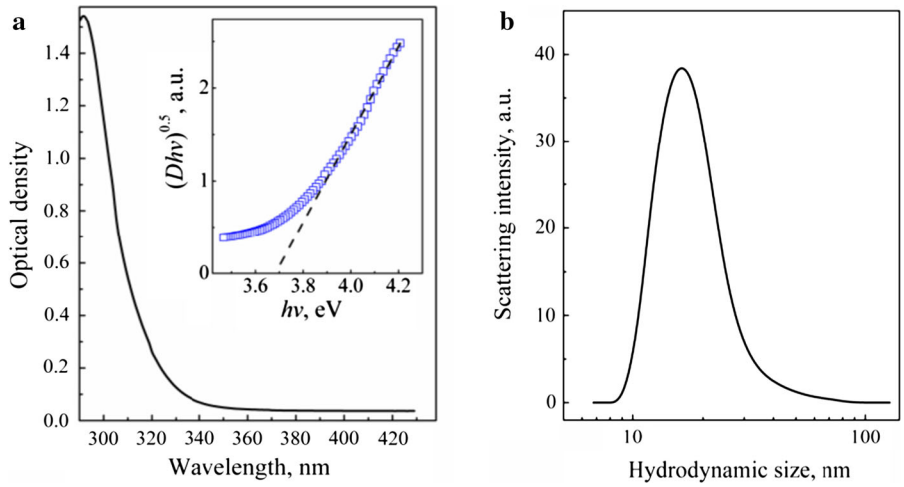

Fig. 1 **a** Absorption spectrum of colloidal MA-stabilized In_2S_3 NPs. Cuvette—10.0 mm. *Inset* in (**a**): the spectrum presented in the coordinates "$(D \times hv)^{0.5}$—hv". **b** Hydrodynamic size distribution of MA-stabilized In_2S_3 NPs in water

polycrystalline NP ensemble with the interplane distances of 2.90, 2.05, 1.90, 1.40, 1.20, 1.05, 0.80, and 0.70 Å typical for the tetragonal β-In_2S_3 phase (Nagesha et al. 2001; Park et al. 2006). Besides, the SAED shows reflections at 1.90, 1.55, and 1.10 Å belonging to α-In_2S_3 and a reflection at 2.80 Å indicating the presence of InS phase (Nagesha et al. 2001). For the α-In_2S_3 and InS phases, the listed reflections are the most intense ones. The rest of the less-intense signals typical for these phases cannot be distinguished in the SAED pattern indicating their presence only as admixtures to the β-In_2S_3 phase. The MA-stabilized In_2S_3 NPs are therefore crystallized predominantly in the tetragonal modification stable at room temperature. The InS admixture forms most probably as a result of partial reduction of In(III) by sulfide ions and MA anions competing with formation of In_2S_3 NPs.

The average size of indium(III) sulfide NPs determined from the dark-field TEM, 20–25 nm (Fig. S1c), corresponds well to the size derived from the bright-field TEM images attesting to predominantly crystalline character of In_2S_3 NPs.

The MA-stabilized In_2S_3 NPs in water and glycerol are characterized by a hydrodynamic size varying in the range of 10–30 nm with a distribution maximum at 15–16 nm (Fig. 1b) as determined by the dynamic light-scattering spectroscopy. The DLS results corroborate the TEM data and confirm that In_2S_3 NPs observed on TEM grids are actually present in original colloidal solutions and do not represent any possible product of re-crystallization induced by the sample drying during the preparation of the TEM samples.

Effect of silver(I) content on optical and PL properties of colloidal Ag–In–S NPs

Doping of the In_2S_3 NPs with Ag^I results in a pronounced "red" shift of the absorption band edge of the colloidal solutions both in water (Fig. 2a) and glycerol as well as in an increase of the integral absorbance of the NPs (Fig. 2a, inset). Even at the minimal Ag^I content corresponding to the molar Ag:In ratio of 1:40 (Fig. 2a, curve 1), the absorption band edge of Ag–In–S NPs is shifted for about 100 nm toward longer wavelengths as compared to undoped indium(III) sulfide NPs (compare Figs. 1a and 2a, curve 1).

Elevation of the dopant content induces further bathochromic shift of the absorption band edge of colloidal solutions and a change in the band shape. The undoped In_2S_3 NPs and Ag–In–S NPs with a small Ag^I amount show relatively low light absorbance at $\lambda > 400$ nm (Fig. 2a, curve 1). With increasing of the silver(I) content, the absorbance of Ag–In–S NPs in this range also increases proportionally (curves 2–5), and at Ag:In > 1:4 both spectral components form almost continuous band with no noticeable bends or shoulders (curves 6, 7). Inset in Fig. 2a shows that the growth of silver(I) content and a decrease of the

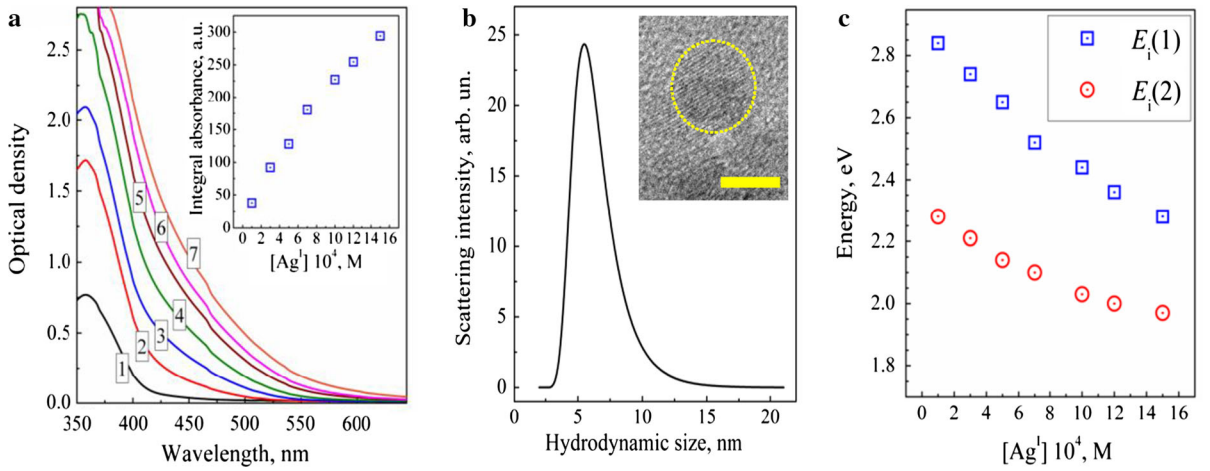

Fig. 2 **a** Absorption spectra of Ag–In–S NPs synthesized at the molar Ag:In ratios of 1:40 (*curve 1*), 1:13 (*2*), 1:8 (*3*), 1:5.7 (*4*), 1:4 (*5*), 1:3.3 (*6*), and 1:2.7 (*7*). Cuvette—10.0 mm. *Inset*: integral absorbance of Ag–In–S colloid at $\lambda > 350$ nm as a function of molar Ag^I content. **b** Hydrodynamic size distribution of freshly prepared Ag–In–S NPs synthesized in water at a molar Ag:In ratio of 1:4. *Inset*: HRTEM image of an Ag–In–S NP, *scale bar* is 5 nm. **c** Energies of indirect interband transitions in Ag–In–S NPs as a function of molar Ag^I content at $[In_2S_3] = 2 \times 10^{-3}$ M, [MAA] = 1.5×10^{-2} M, and [NaOH] = 1.5×10^{-2} M

Ag:In ratio from 1:40 to 1:2.7 result in an almost 6-time increment of the integral absorbance of Ag–In–S NPs at $\lambda > 400$ nm.

Dynamic light-scattering measurements showed that the average hydrodynamic size of freshly prepared Ag–In–S NPs is typically smaller than 10 nm in the entire Ag(I) content range studied. For example, at a molar Ag:In ratio of 1:4, the average hydrodynamic size of Ag–In–S NPs is 5–6 nm (Fig. 2b). Similar result was obtained by HRTEM (see example in the inset of Fig. 2b). The interplanar distance visible on the HRTEM image, ~2.05 Å, is typical for tetragonal β-In_2S_3, indicating that the lattice parameters of indium sulfide NPs remain unchanged upon the doping with Ag(I) ions. The SAED pattern of Ag–In–S NPs produced at Ag:In = 1:4 (ESM, Fig. S2a) shows concentric reflections corresponding to the interplanar distances of 1.05, 1.20, and 2.05 Å, characteristic for β-In_2S_3.

Analysis of the absorption spectra of Ag–In–S NPs at Ag:In > 1:40 using the Tauc equation revealed two distinct linear sections of the $(D \times h\nu)^{0.5}$–$h\nu$ relationships corresponding apparently to two indirect interband electron transitions with a different E_i parameter (ESM, Fig. S2b). It should be noted that at any given silver(I) content in the range studied the absorption spectrum of Ag–In–S NPs differs distinctly by the spectral parameters and band intensity from the absorption spectrum of a mixture of separate In_2S_3 and Ag_2S NPs with the same content and molar ratio of Ag and In. The fact shows that the absorption spectra presented in Fig. 2a belong to the Ag–In–S NPs and are not a superposition of the absorption spectra of a mixture of In_2S_3 and Ag_2S NPs.

In fact, it was found earlier that the absorption band edge of colloidal Ag_2S NPs in water also originates from a combination of two indirect electron transitions (Kryukov et al. 2004). The energies of the transitions in Ag_2S NPs vary in the range of 1.36–1.76 eV (E_i(1)) and 0.90–1.24 eV (E_i(2)) depending on the synthesis conditions (Kryukov et al. 2004). These values are much lower than the indirect transition energies in the case of Ag–In–S NPs—2.19–2.84 eV (E_i(1)) and 1.93–2.22 eV (E_i(2)) supporting the conclusion that no separate Ag_2S phase is present in the Ag–In–S colloids.

Figure 2c shows that the augmentation of the molar Ag^I content in Ag–In–S NPs and the corresponding decrease of the Ag:In ratio result in an almost linear decrease of both energies of the electron transitions. Therefore, doping with Ag^I gives means of tailoring of the photophysical properties of Ag–In–S NPs in a reasonably broad range.

The EDX analysis of Ag–In–S NPs subjected to purification by the dialysis showed that the Ag:In

ratio in the NPs is in all cases very close to the ratio of the metals in the original precursor mixture at the synthesis. For example, for the Ag–In–S NPs produced at an Ag:In ratio of 1:4, the EDX analysis shows the Ag:In ratio varying from 1:3.5 to 1:3.9 depending on the analysis spot (ESM, Fig. S3 and Table S1).

No photoluminescence was detected at the excitation of the In_2S_3 NPs into the absorption band, at $\lambda_{ex} = 300$ nm (Fig. 3a, curve 1), testifying to exclusively radiationless character of the electron–hole recombination in the undoped In_2S_3 NPs. At the same time, doping with even the smallest amount of silver(I) imparts indium(III) sulfide NPs with the photoluminescence emitted in comparatively broad band (curve 2) with a maximum at 575–580 nm (2.14–2.16 eV) and a spectral width of ~100 nm (0.36 eV). At an increase of the Ag^I content and a decrease of the Ag:In ratio from 1:40 to 1:4, the PL intensity grows by a factor of about 2.5. Additionally, the PL band shows a "red" shift of the maximum to 615–620 nm (~2 eV) and a broadening of the band to ~0.5 eV (Fig. 3a, curves 3–6, and Fig. 3b). The quantum yield of PL of Ag–In–S NPs prepared at Ag:In = 1:4 is 12 %. At a smaller Ag:In ratio (Fig. 3a, curves 6, 7), the PL intensity is lower and the band maximum resides at 620–625 nm.

The dependencies of the minimal interband transition energy $E_i(2)$ (Fig. 3c, curve 1) and the energy E_{PL} of the PL band maximum (curve 2) on the silver(I) content in Ag–In–S NPs almost coincide starting from Ag:In ~1:4–5. The Stokes shift that is a difference between $E_i(2)$ and E_{PL} amounts to ~70 meV at the minimal Ag^I content (Ag:In = 1:40) and decreases sharply at an increase of the dopant concentration reaching zero at Ag:In = 1:3.3 (Fig. 3c, inset).

Two basic types of photoluminescence are usually observed for metal chalcogenide NPs including I–III–VI_2 compounds (Li et al. 2010; Hamanaka et al. 2014; Rao et al. 2014; Torimoto et al. 2014): the first one originating from the direct interband electron–hole recombination and the second one involving recombination with the participation of trapped charge carriers. Various lattice defects act as the traps capturing free charge carriers with a loss in electron energy as the corresponding electron levels of the traps reside in the band gap below the conduction band (electron traps) or above the valence band (hole traps). In the former case, the PL band is characterized by a relatively narrow spectral width and a small (or zero) Stokes shift, while in the latter case the PL band shows a considerable Stokes shift (0.5–1.5 eV) and a large spectral width. In that, the band width depends on

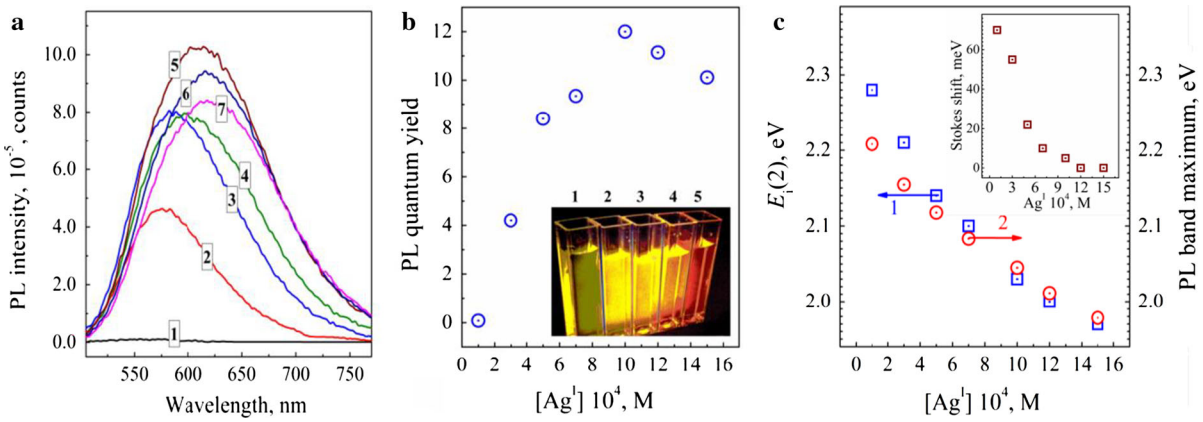

Fig. 3 **a** Photoluminescence spectra of colloidal Ag–In–S NPs synthesized in water at the molar Ag:In ratios of 1:40 (*curve 1*), 1:13 (*2*), 1:8 (*3*), 1:5.7 (*4*), 1:4 (*5*), 1:3.3 (*6*), and 1:2.7 (*7*). **b**, **c** PL quantum yield of Ag–In–S NPs (**b**), $E_i(2)$ energy (**c**, *curve 1*), and PL band maximum energy (**c**, *curve 2*) as a function of molar Ag^I content. *Inset* in **b**: Photograph of cuvettes with Ag–In–S colloids synthesized at the Ag:In ratios of 1:40 (*1*), 1:13 (*2*), 1:4 (*3*), 1:3.3 (*4*), and 1:2.7 (*5*) and illuminated with UV light (λ = 310–370 nm). *Inset* in **c**: Stokes shift of PL band as a function of Ag^I content. $[In_2S_3] = 2 \times 10^{-3}$ M, [MAA] = 1.5×10^{-2} M, and [NaOH] = 1.5×10^{-2} M

distributions of the traps by the energy and by the distance between the electron and hole traps, as well as a distribution of NPs by the size in the range where a size dependence of the bandgap is observed for the given semiconductor. Only the latter factor typically contributes to the spectral width of the PL band in the case of direct radiative electron–hole recombination.

A relatively small or zero Stokes shift observed at a high silver(I) content in the Ag–In–S NPs indicates that the PL of Ag–In–S NPs originates from the direct radiative recombination of photogenerated charge carriers. At the same time, the Ag–In–S NPs demonstrate quite a high spectral width of the PL band that is not typical for the direct recombination in metal chalcogenide semiconductors. It should be noted that for the most broadly studied chalcogenide luminophores, such as CdX and ZnX, the Bohr radius a_B of the exciton is smaller than 10 nm, and therefore the spatial exciton confinement and size dependence of the bandgap are negligible for larger NPs. In the case of indium(III) sulfide, a_B is as high as ~30 nm, so the strong spatial confinement of exciton and a strong size dependence of the bandgap and the PL band maximum could be envisaged for In_2S_3 and Ag–In–S NPs. A large, ~1.7 eV, "blue" shift of the absorbance threshold of colloidal In_2S_3 NPs as compared to the bulk indium(III) sulfide is a vivid evidence of such a strong quantum size effect. Therefore, for the ensemble of 5–6-nm Ag–In–S NPs, a large difference between the PL band maxima of the smallest and the largest NPs could be expected contributing to an unusually large spectral width of the PL band.

Effect of thermal treatment on optical and PL properties of colloidal Ag–In–S NPs

The MA-stabilized Ag–In–S NPs in water and glycerol retain stability to aggregation at any silver(I) amount both at room temperature and when kept for a long time at boiling T in water or at 120–130 °C in the case of glycerol.

Figure 4a illustrates heating-induced evolution of the PL properties of Ag–In–S NPs in glycerol at Ag:In = 1:4, that is for the NPs with the highest PL intensity observed prior to the thermal treatment. Incubation of the colloid at 120 °C for 40 min induces a bathochromic shift of the PL band maximum from 615–620 nm (Fig. 4a, curve 1) to 760–765 nm (Fig. 4a, curve 9). So, a combination of two factors—variation of the Ag^I content and adjustment of the duration of the thermal treatment—can be used to vary the position of the PL band maximum in the scope of around 200 nm—from 575–580 to 760–765 nm. In such a way, the luminophores with a broad palette of emission colors—from orange to dark-red—can be produced (see photographs in Figs. 3b and 4a).

The thermal treatment of colloidal Ag–In–S in glycerol for 25 min results in a fourfold amplification of the PL intensity (Fig. 4a). However, at a longer exposure at 120 °C the PL efficiency lowers. An increase of PL intensity coupled with a "red" shift of the PL band maximum is a typical phenomenon for nanosized metal chalcogenide luminophores subjected to thermal treatment. The PL efficiency increase is usually interpreted in terms of annealing of the structural defects and a decrease of the lattice disorder resulting in a lower efficiency of the radiationless electron–hole recombination. The "red" shift of the PL maximum is caused by the Ostwald ripening—enlargement of larger NPs at the expense of the mass transfer from smaller NPs that are more soluble and gradually vanish. The NP size increase results in the relaxation of the spatial confinement of the photogenerated charge carriers and a narrowing of the size-dependent bandgap. Realization of this scenario in the system under study is confirmed by a lowering of the $E_i(2)$ and E_{PL} energies as well as a narrowing of the PL band from 0.5 eV before the thermal treatment to 0.3 eV after the aging at 120 °C. As the spectral width of the PL band is determined mostly by the size distribution of Ag–In–S NPs, the narrowing of the PL band points on the narrowing of the NP size distribution as a result of vanishing of a fraction of smaller NPs.

The above assumption about the NP size increase induced by the thermal treatment is supported by the dynamic light-scattering measurements. The DLS data indicate that even relatively short (~10 min) exposure of Ag–In–S NPs in glycerol to heating at 120 °C results in an NP size increase from 5–6 nm in the as-prepared colloids to ~40 nm (compare Fig. 1b and curve 1 in Fig. 4b). The DLS results are corroborated by SEM data (ESM, Fig. S4) showing that the average hydrodynamic size of Ag–In–S NPs at this stage of heating is 20–30 nm. Resuming of the heating results in further growth of the Ag–In–S NP size (Fig. 4b), and after 60–70 min the average hydrodynamic size of

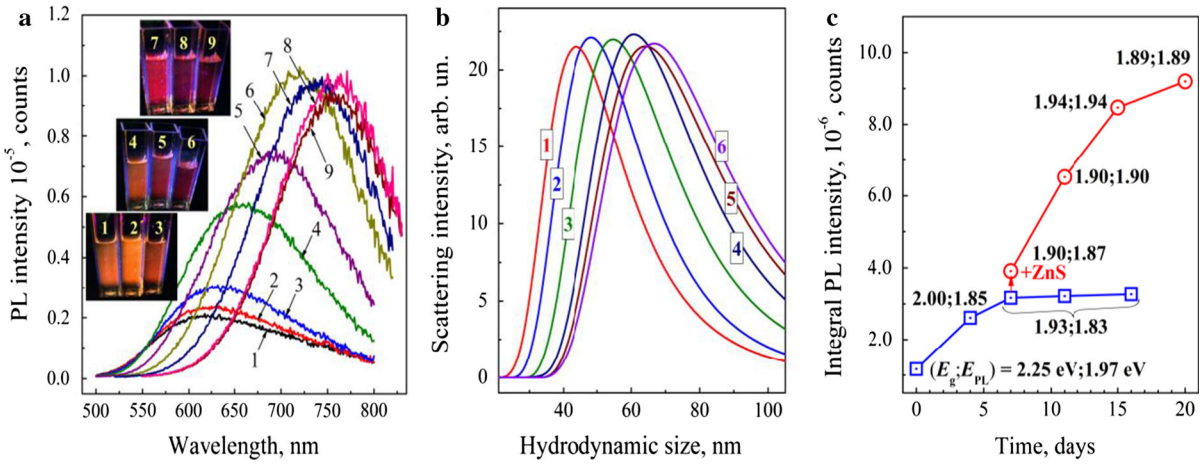

Fig. 4 **a** Photoluminescence spectra and photographs of colloidal Ag–In–S NPs prepared in glycerol at Ag:In = 1:4 immediately after the synthesis (*curve 1*) and after thermal treatment at 120 °C for 5 min (*2*), 10 min (*3*), 15 min (*4*), 20 min (*5*), 25 min (*6*), 30 min (*7*), 35 min (*8*), and 40 min (*9*). **b** Hydrodynamic size of Ag–In–S NPs prepared at Ag:In = 1:4 after thermal treatment at 120 °C for 10 (*1*), 20 (*2*), 30 (*3*), 40 (*4*), 60 (*5*), and 70 min (*6*). **c** Integral PL intensity of Ag–In–S NPs in water aged at room *T* for 7 days, then modified with a ZnS shell (the moment marked by an *arrow*) and aged for additional 20 days. The corresponding values of $E_i(2)$ and E_{PL} are given for each point on the figure. $[In_2S_3] = 2 \times 10^{-3}$ M, [MAA] = 1.5×10^{-2} M, and [NaOH] = 1.5×10^{-2} M

Ag–In–S NPs increases to 65–70 nm (Fig. 4b, curves 5, 6). The EDX analysis of Ag–In–S NPs produced by heating for 70 min showed that the Ag:In ratio in the NPs remains the same as for the original as-prepared NPs, indicating that aging at the elevated temperature does not affect the composition of Ag–In–S NPs (ESM, Fig. S3b and Table S1).

Alternatively to the thermal treatment, the optical and PL properties of colloidal Ag–In–S NPs can be tailored by a prolonged aging at room temperature and/or deposition of a ZnS layer on the surface of Ag–In–S NPs. Aging of the aqueous Ag–In–S colloid at 18–20 °C for 7 days results in a decrease of $E_i(2)$ and E_{PL} from 2.25 and 1.97 to 1.93 and 1.83 eV, respectively, indicating an increase of the NP size. In that, the integral PL intensity increases by about three times (squares on Fig. 4c). No further changes of the characteristics of absorption and PL bands as well as the PL intensity were observed at a more prolonged aging at room T, up to 20 days. The quantum PL yield of Ag–In–S NPs incubated at room T for this period of time is 12 % at Ag:In = 1:4. Similar result was achieved by the thermal treatment of the colloids at ~100 °C for 15 min.

Recently, we have found that the PL efficiency of CdSe NPs stabilized in aqueous colloids can be boosted by the deposition of a wider bandgap ZnS "shell" (Dzhagan et al. 2008, 2009). Formation of the ZnS layer on the surface of CdSe NPs resulted in an almost twofold increase of the PL efficiency as a result of passivation of surface defects. It was found that the similar effect is observed after deposition of a ZnS layer on the surface of Ag–In–S NPs (a moment of transition from squares to circles denoted by an arrow in Fig. 4b). Contrary to the uncovered Ag–In–S NPs, the "core/shell" Ag–In–S/ZnS NPs exhibit a steady growth of the PL intensity for a much longer time. After 15–20-day aging at room T, the PL efficiency increases by a factor of 8–9 (circles in Fig. 4b) as compared to the freshly prepared Ag–In–S NPs. The quantum PL yield of Ag–In–S/ZnS NPs reaches ~30 %. A "blue shift" of the PL maximum from 1.83 to 1.87 eV (Fig. 4c) observed after the ZnS shell deposition can be explained by Zn migration from the shell material into the Ag–In–S core with the formation of alloyed zinc-containing phases (Torimoto et al. 2010, 2014; Xiang et al. 2014).

Similarly to the case of thermal treatment of Ag–In–S NPs, the room-T aging of Ag–In–S/ZnS NPs for a period longer than 10 day also results in diminishing of the Stokes shifts to zero (compare $E_i(2)$ and E_{PL} given in Fig. 4b) indicating on the direct

(interband) character of the radiative electron–hole recombination in the Ag–In–S/ZnS NPs.

Time-resolved PL spectroscopy of Ag–In–S NPs

The kinetic curves of PL decay of colloidal Ag–In–S NPs have a complex shape (Fig. 5a) and can be approximated by linear combinations of at least three monoexponential functions. An increase in the silver(I) content in Ag–In–S NPs results in a slowing of the PL decay (Fig. 5a) and an increase of the average radiative NP life-time $<\tau>$ (Fig. 5b). In particular, the reduction of the molar Ag:In ratio from 1:20 to 1:4 results in a twofold $<\tau>$ increase—from 480 to 960 ns (colloidal NPs were synthesized in glycerol and subjected to the thermal treatment at 120 °C for 20 min prior to the kinetic measurements). Complete PL extinction is observed only in 5–6 μs after the photoexcitation. A further increase in the Ag^I content results in some lowering of the radiative life-time (Fig. 5b) pointing on the participation of silver ions in the radiationless processes. In general, the dependence

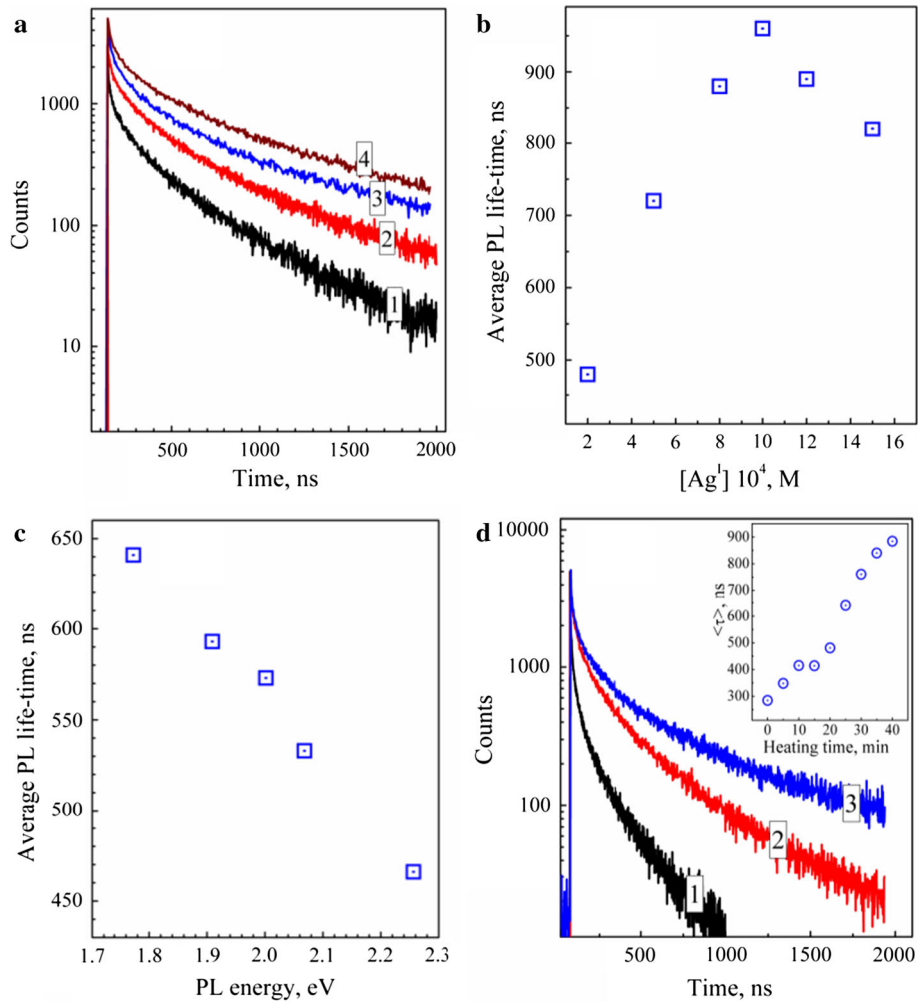

Fig. 5 **a** Kinetic curves of PL decay of Ag–In–S NPs prepared in glycerol at Ag:In = 1:20 (*curve 1*), 1:8 (*2*), 1:4 (*3*), and 1:2.7 (*4*). **b**, **c** Average PL life-time $<\tau>$ of Ag–In–S NPs as a function of **b** silver(I) content and **c** PL quantum energy. **d** Kinetic curves of PL decay of Ag–In–S NPs synthesized at Ag:In = 1:4 at room T (*curve 1*, registered at $\lambda_{reg} = 620$ nm) and after thermal treatment at 120 °C for 20 min (*curve 2*, $\lambda_{reg} = 680$ nm) and 40 min (*curve 3*, $\lambda_{reg} = 760$ nm). *Inset*: $<\tau>$ as a function of thermal treatment time at 120 °C. In **c** and **d** Ag:In = 1:4. Colloid composition: $[In_2S_3] = 2 \times 10^{-3}$ M, [MAA] = 1.5×10^{-2} M, and [NaOH] = 1.5×10^{-2} M

between $<\tau>$ and the dopant content presented in Fig. 5b resembles the dependence of the stationary PL band intensity on the concentration of silver(I) in the Ag–In–S NPs (see Fig. 3b). The kinetic parameters of the PL decay are almost identical for the Ag–In–S NPs synthesized in water and glycerol in the same conditions.

Within the spectral scope of the PL band, the kinetics of PL decay depends on the recording wavelength and, therefore, on the PL quantum energy. For example, the life-time $<\tau>$ of Ag–In–S NPs synthesized at Ag:In = 1:4 increases from ~470 to 640 ns at a decrease in the quantum energy from 2.26 to 1.77 eV (Fig. 5c). Taking into account the size-dependent bandgap distribution in an ensemble of Ag–In–S NPs, such behavior can be interpreted in terms of the size dependence of the rate of radiative electron–hole recombination. In that, the smaller NPs emit PL with a larger energy (which is equal to the bandgap of such NPs) faster than the NPs of larger size.

The polyexponential character of the kinetic curves and a dependence of the recombination rate on the PL energy are often reported for metal chalcogenide NPs, including the I–III–VI_2 group (Tang et al. 2012; Liu et al. 2013; Hamanaka et al. 2014; Rao et al. 2014; Xiang et al. 2014). These phenomena are generally associated with the size distribution in the NP ensemble and a size dependence of the rate of radiative electron–hole recombination. Similar model is proposed also to explain the relationship between the PL quantum energy and the average life-time of the photoexcited NPs.

Thermal treatment of silver(I)-doped indium(III) sulfide colloids was found to affect not only the stationary PL properties but also the dynamics of PL decay of Ag–In–S NPs (Fig. 5d). In particular, the Ag–In–S NPs synthesized in glycerol at Ag:In = 1:4 and room T are characterized by $<\tau>$ ~280 ns (Fig. 5d, inset). Annealing of colloids at 120 °C results in an increase of the average life-time of Ag–In–S NPs proportional to the duration of the thermal treatment. In such a way, $<\tau>$ increases in more than 3 times—to 880 nm after 40-min thermal treatment (Fig. 5d, inset). The considerable increase of the radiative NP life-time speaks decisively in favor of the above assumption about ordering of the NP lattice during the thermal treatment and elimination of the lattice defects acting as charge carrier traps and centers of the radiationless electron–hole recombination.

Conclusion

A synthesis of stable colloidal solutions of indium(III) sulfide stabilized by mercaptoacetate in water and glycerol is reported. The colloids contain crystalline particles of tetragonal β-In_2S_3 with a size of 15–30 nm exhibiting quantum size effects, in particular a considerable "blue" shift of the absorption band edge as compared to the bulk counterpart.

Doping of the non-luminescing In_2S_3 with Ag^I ions during the synthesis results in the formation of the non-stoichiometric Ag–In–S NPs with the photoluminescence in the visible part of the spectrum as well as a "red" shift of the absorbance threshold and the PL band maximum position proportional to the dopant concentration. According to the EDX analysis of Ag–In–S NPs purified by dialysis, the Ag:In ratio in the NPs corresponds closely to the molar ratio of Ag(I) and In(III) in the starting precursors.

The spectral parameters of the absorption and PL bands of Ag–In–S NPs synthesized in water and glycerol in the same conditions are identical. At a higher Ag^I content, the emission band of Ag–In–S NPs is characterized by a small or zero Stokes shift of the PL band maximum energy relative to the minimal interband transition energy. The fact allows to assign the PL emission to the direct interband radiative electron–hole recombination. The highest PL quantum yield, 12 %, is observed at a molar Ag:In ratio of 1:4. Deposition of a ZnS "shell" on the surface of "core" Ag–In–S NPs results in an increase of the PL quantum yield to ~30 %.

The thermal treatment of Ag–In–S colloids at 100 °C (water) or 120 °C (glycerol) results in a "red" shift of the PL band maximum and an increase in the PL intensity. Simultaneously, a lowering of the interband electron transition energy is observed indicating that the average size of Ag–In–S NPs grows during the thermal treatment. The conclusion is corroborated by an increase of the average hydrodynamic size of Ag–In–S NPs from 5–6 nm before the thermal treatment to 65–70 nm after 60–70 min of aging at 120 °C. Varying the silver(I) content and the thermal treatment duration, the PL band maximum position of Ag–In–S NPs can be shifted in a controlled way from 575–580 to 760–765 nm allowing to produce luminophores emitting a broad gamma of light—from orange to dark-red.

The kinetic curves of PL decay of Ag–In–S NPs have a distinct polyexponential character. The average

radiative life-time of the excited Ag–In–S NPs depends on the silver(I) content and reaches the maximal value of 960 ns at a molar Ag:In ratio of 1:4. A considerable increase of the radiative life-time induced by the thermal treatment of Ag–In–S colloids was interpreted in terms of annealing of the structural defects acting as centers of the radiationless electron–hole recombination.

Acknowledgments Authors thank Dr. I. Kotenko (L.V. Pysarzhevsky Institute of Physical Chemistry of NASU, Kyiv, Ukraine) and Dr. S. Schulze (Institute of Physics, Technical University of Chemnitz, Germany) for TEM and SAED results and M. Skoryk (LLC Nanomedtech, Kyiv, Ukraine) for SEM and EDX data. The financial support of State Fund for Fundamental Research of Ukraine (Project No. Ф53.3/019) and National Academy of Sciences of Ukraine (Joint Projects of NASU and Siberian Branch of RAS Nos 07-03-12 Ukr and 49-02-14(U)) is acknowledged.

References

Chang W, Wu C, Jeng M, Cheng K, Huang C, Lee T (2010) Ternary Ag–In–S polycrystalline films deposited using chemical bath deposition for photoelectrochemical applications. Mater Chem Phys 120:307–312

Chang J, Wang G, Cheng C, Lin W, Hsu J (2012) Strategies for photoluminescence enhancement of $AgInS_2$ quantum dots and their application as bioimaging probes. J Mater Chem 22:10609–10618

Chen W, Bovin J, Joly A, Wang S, Su F, Li G (2004) Full-color emission from In_2S_3 and In_2S_3: Eu^{3+} nanoparticles. J Phys Chem B 108:11927–11934

Du W, Qian X, Yin J, Gong Q (2007) Shape- and phase-controlled synthesis of monodisperse, single-crystalline ternary chalcogenide colloids through a convenient solution synthesis strategy. Chem Eur J 13:8840–8846

Dzhagan V, Valakh M, Raevskaya A, Stroyuk A, Kuchmiy S, Zahn (2008) Characterization of semiconductor core–shell nanoparticles by resonant Raman scattering and photoluminescence spectroscopy. Appl Surf Sci 255:725–727

Dzhagan V, Valakh M, Raevskaya A, Stroyuk O, Kuchmiy S, Zahn D (2009) The influence of shell parameters on phonons in core–shell nanoparticles: a resonant Raman study. Nanotechnol 20:365704

Hamanaka Y, Ozawa K, Kuzuya T (2014) Enhancement of donor–acceptor pair emissions in colloidal $AgInS_2$ quantum dots with high concentration of defects. J Phys Chem C 118:14562–14568

Han J, Liu Z, Guo K, Ya J, Zhao Y, Zhang X, Hong T, Liu J (2014) High-efficiency $AgInS_2$-modified ZnO nanotube array photoelectrodes for all-solid-state hybrid solar cells. ACS Appl Mater Interfaces 6:17119–17125

Kamat P, Tvrdy K, Baker D, Radich J (2010) Beyond photovoltaics: semiconductor nanoarchitectures for liquid-junction solar cells. Chem Rev 110:6664–6688

Klostranec J, Chan W (2006) Quantum dots in biological and biomedical research: recent progress and present challenges. Adv Mater 18:1953–1964

Kolny-Olesiak J, Weller H (2013) Synthesis and application of colloidal $CuInS_2$ semiconductor nanocrystals. ACS Appl Mater Interfaces 5:12221–12237

Kryukov A, Zinchuk N, Korzhak A, Stroyuk A, Kuchmiy S (2004) Optical and catalytic properties of Ag_2S nanoparticles. J Mol Catal A 221:209–221

Li X, Niu J, Shen H, Xu W, Wang H, Li L (2010) Shape controlled synthesis of tadpole-like and heliotrope seed-like $AgInS_2$ nanocrystals. CrystEngComm 12:4410–4415

Li K, Xu J, Zhang X, Peng T, Li X (2013) Low-temperature preparation of $AgIn_5S_8/TiO_2$ heterojunction nanocomposite with efficient visible-light-driven hydrogen production. Inter J Hydrog Energy 38:15965–15975

Liu L, Hu R, Law W, Roy I, Zhu J, Ye L, Hu S, Zhang X, Yong K (2013) Optimizing the synthesis of red- and near-infrared $CuInS_2$ and $AgInS_2$ semiconductor nanocrystals for bioimaging. Analyst 138:6144–6153

Nagesha D, Liang X, Mamedov A, Gainer G, Eastman M, Giersig M, Song J, Ni T, Kotov N (2001) In_2S_3 nanocolloids with excitonic emission: In_2S_3 vs CdS comparative study of optical and structural characteristics. J Phys Chem B 105:7490–7498

Park K, Jang K, Son S (2006) Synthesis, optical properties, and self-assembly of ultrathin hexagonal In_2S_3 nanoplates. Angew Chem Int Ed 45:4608–4612

Peng E, Choo E, Tan C, Tang X, Sheng Y, Xue J (2013) Multifunctional PEGylated nanoclusters for biomedical applications. Nanoscale 5:5994–6005

Rao M, Shibata T, Chattopadhyay S, Nag A (2014) Origin of photoluminescence and XAFS study of $(ZnS)_{1-x}(AgInS_2)_x$ Nanocrystals. J Phys Chem Lett 5:167–173

Rühle S, Shalom M, Zaban A (2010) Quantum-dot-sensitized solar cells. ChemPhysChem 11:2290–2304

Sasamura T, Okazaki K, Kudo A, Kuwabata S, Torimoto T (2012) Photosensitization of ZnO rod electrodes with $AgInS_2$ nanoparticles and ZnS-$AgInS_2$ solid solution nanoparticles for solar cell applications. RSC Adv 2:552–559

Talapin D, Lee J, Kovalenko M, Shevchenko E (2010) Prospects of colloidal nanocrystals for electronic and optoelectronic applications. Chem Rev 110:389–458

Tang X, Ho W, Xue J (2012) Synthesis of Zn-doped $AgInS_2$ nanocrystals and their fluorescence properties. J Phys Chem C 116:9769–9773

Tian L, Vittal J (2007) Synthesis and characterization of ternary $AgInS_2$ nanocrystals by dual- and multiple-source methods. New J Chem 31:2083–2087

Torimoto T, Ogawa S, Adachi T, Kameyama T, Okazaki K, Shibayama T, Kudo A, Kuwabata S (2010) Remarkable photoluminescence enhancement of ZnS–$AgInS_2$ solid solution nanoparticles by post-synthesis treatment. Chem Commun 46:2082–2084

Torimoto T, Tada M, Dai M, Kameyama T, Suzuki S, Kuwabata S (2012) Tunable photo-electrochemical properties of chalcopyrite $AgInS_2$ nanoparticles size-controlled with a photoetching technique. J Phys Chem C 116:21895–21902

Torimoto T, Kameyama T, Kuwabata S (2014) Photofunctional materials fabricated with chalcopyrite-type semiconductor

nanoparticles composed of $AgInS_2$ and its solid solutions. J Phys Chem Lett 5:336–347

Xiang W, Xie C, Wang J, Zhong J, Liang X, Yang H, Luo L, Chen Z (2014) Studies of highly luminescent $AgInS_2$ and Ag–Zn–In–S quantum dots. J Alloys Compd 588:114–121

Xiong W, Yang G, Wu X, Zhu J (2013) Microwave-assisted synthesis of highly luminescent $AgInS_2$/ZnS nanocrystals for dynamic intracellular Cu(II) detection. J Mater Chem 1:4160–41659

Yin J, Jia J, Yi G (2013) Synthesis and photoelectric applications of $AgInS_2$ clusters. Mater Lett 111:85–88

Zhang W, Li D, Chen Z, Sun M, Li W, Lin Q, Fu X (2011) Microwave hydrothermal synthesis of $AgInS_2$ with visible light photocatalytic activity. Mater Res Bull 46:975–982

Zhong H, Bai Z, Zou B (2012) Tuning the luminescence properties of colloidal I–III–VI semiconductor nanocrystals for optoelectronics and biotechnology applications. J Phys Chem Lett 3:3167–3175